Pore structure characteristics of low- and medium-rank coals and their differential adsorption and desorption effects

Boyang Wang [a,b,*], Yong Qin [a,b], Jian Shen [a,b], Qiusheng Zhang [c], Gang Wang [d]

[a] Key Laboratory of Coalbed Methane Resources and Reservoir Formation Process of the Ministry of Education, China University of Mining and Technology, Xuzhou, Jiangsu 221008, China
[b] School of Resources and Geosciences, China University of Mining and Technology, Xuzhou, 221116, China
[c] Suzhou NanZee Sensing Technology Co. Ltd., Suzhou 215123, China
[d] School of Earth Science and Engineering, Hebei University of Engineering, 056038, China

ABSTRACT

The pores and methane adsorption-desorption characteristics are different between low- and medium-rank coal. For this paper, mercury intrusion porosimetry and isothermal adsorption experiments were carried out on thirteen coal samples with $R_{o,max}$ between 0.22% and 0.98%. To evaluate the effect of the pore structure on coal permeability, we calculated the multi-scale fractal dimensions according to classic geometry models and discussed factors influencing pore fractals, including metamorphism degree, ash yield, and the content of vitrinite (huminite). Three key pressures in the stage of depressurization were calculated on the basis of Langmuir adsorption theory, and the influencing factors were discussed, including metamorphism degree, fractal dimension, and moisture content. The results show that pores of the coal can be divided into three types according to the pore diameter boundaries of 6,000 nm and 100 nm. The multi-scale fractal dimensions of coal pores (D_1, D_2, D_3) are in the range of 2.341–2.836, 2.041 to 2.476, 2.237 to 2.656, respectively. The pore fractal dimension (D_1) is controlled by the degree of metamorphism, and D_3 is mainly affected by ash yield, the content of vitrinite (huminite), and the degree of metamorphism. The adsorption of low- and medium-rank coal is a step-by-step control mode under the control of coal metamorphism, in which lignite mainly depends on the moisture content, and long-flame coal-gas coal mainly depends on the adsorption-diffusion hole (<100 nm) pore structure. The lower the fractal dimension of adsorption pore, the better the adsorption. The higher the fractal dimension of the seepage pore, the better the seepage. Four desorption stages of the desorption process are subdivided according to three critical pressure points (starting pressure, transition pressure, and depletion pressure). The different critical pressure points are mainly affected by the degree of coal metamorphism, the pore structure characteristics of the primary seepage pore, and the moisture content. Larger Langmuir volume (V_L) and ratio of Langmuir constants ($1/P_L$) are beneficial to earlier advent of steady production stage, whereas it is also possible that the declining production stage may occur ahead of schedule.

1. Introduction

According to the 13th five-year plan and the overall goal of China's coal bed methane (CBM) industry to be completed in 2020, the focus of CBM exploration has shifted from using high-rank coals to low- and medium-rank coals. The resources of low- and medium-rank CBM are about 14.7 trillion, accounting for about 43% of the total CBM resources in China (Ye et al., 2009). Although many low- and medium-rank coal basins have achieved a breakthrough in CBM productivity and show broad prospects, such as Ordos Basin, Yilan Basin, and so on, commercial

development has been unsuccessful. One of the important reasons is that there is no deep understanding of the relationship between the composition, the pore characteristics, and the characteristics of coal adsorption and desorption of low- and medium-rank coals (Jian et al., 2015).

At present, the influence of the coal composition on the pore distribution and adsorption capacity is still controversial, and the influence of pore distribution and structure characteristics on adsorption, desorption, and seepage have not yet been determined, which is mainly controlled by the coal rank (Laxminarayana and Crosdale, 1999; Clarkson and Bustin, 2000; Deng et al., 2015; Zhou et al., 2017a; Fu et al., 2017). Some

scholars attempted to compare and analyze the pore distribution characteristics of different rank coals and their influence on adsorption-desorption-diffusion, but more research has been performed regarding coal at the two terminal of the degree of coal metamorphism (Keshavarz et al., 2017; Peng et al., 2017). Few scholars have studied the material composition, pore characteristics, adsorption and desorption characteristics of low- and medium-rank coals before and after the first jump point ($R_{o,max} = 0.6\%$).

Coal pores are distributed in a three-dimensional space, and it is hard to precisely reflect the heterogeneity of coal reservoirs using traditional geometric methods (Zhang et al., 2009). The concept of fractals was proposed by Mandelbrot in 1975 to assess the real properties and states of porous materials (Li et al., 2016). Previous studies have concluded that coal has obvious fractal features at different scales (Fu et al., 2017). Most of the former achievements have focused on the fractal features of high rank coal within a certain range of pore diameter (Cai et al., 2011; Zhang et al., 2014). There has been no systematic study of the fractal features of low- and medium-rank coal within the full aperture. Different pore scales have different effects on the adsorption and seepage capacity of coal, and previous studies have considered that the macro-pore (>1000 nm) and the meso-pore (100–1000 nm) is a seepage pore; the transitional-pore (10–100 nm) and micro-pore (<10 nm) is an adsorption pore, as the porosity is classified according to the Hodot's decimal pore structure classification system (Hodot, 1966; White et al., 2005; Hou et al., 2012; Liu et al., 2015; Meng et al., 2016). Some scholars have attempted to study the full-scale pore fractal fractures using low-temperature liquid nitrogen, high-pressure mercury, and nuclear magnetic resonance (Zhou et al., 2017b). Overall, the fractal theory provides new ideas for the study of methane adsorption, desorption and seepage by quantifying the microscopic pore structure of coal reservoirs. However, the influence of the fractal characteristics on the adsorption-desorption- seepage of the low- and medium-rank coal has not been fully studied.

Based on this, different rank coals are collected from 11 coal mines throughout China to conduct industrial analysis, maceral quantitative analysis, the mercury intrusion test, and the equilibrium moisture isothermal adsorption test. Based on fractal theories, the fractal dimensions at different scales were calculated. D_1, D_2, and D_3 corresponded to pore-size ranges of larger than 6000 nm, 100 nm-6000 nm and 3 nm-100 nm, respectively. First, we discussed the relationships between the fractal dimensions and coal rank, coal composition and pore structure parameters. Subsequently, the impact of the fractal dimensions on the methane adsorption and desorption were discussed. Then, differences of

adsorption and desorption characteristics between low and medium rank coals were also compared. This research will be useful for understanding the pore structure of low and medium rank coals and has practical significance for CBM exploration in China.

2. Coal sample, experiment, and data processing method

2.1. Coal samples and experimental methods

Coal samples from 11 coal mines throughout China and their respective sampling points are shown in Fig. 1. According to the different types of coal, 13 representative coal samples are chosen for this study, and the output information of the coal samples is shown in Table 1.

The maximum reflectivity of the vitrinite and the quantitative statistics of coal macerals were determined by optical microscope under the condition of oil immersion reflection light according to the national standard GB/T6948-2008. Industrial analysis is completed in accordance with GB/T 202-2008. The basic parameters of the coal sample are shown in Table 2.

The apparent relative density and true relative density of coal are tested to calculate the porosity of the coal according to the national standards of GB/T 217-2008 and GB/T 217-1998, respectively. The pore structure analysis of coal was performed using an Auto Pore IV 9 510 type automatic mercury pressure apparatus. The contact angle between the mercury and the coal surface was 140°, the surface tension of mercury was 480 dyn/cm, and the pore diameter range was larger than 3.0 nm. The permeability was tested using a PDP-200 Krystal pulse attenuation permeability meter. The pore structure is divided by a decimal aperture structure classification system. Statistics of coal specific pore volume and specific surface distribution for macro-pore (>1000 nm), meso-pore (100–1000 nm), transition pore (10–100 nm), and micro-pore (<10 nm) were acquired (Tables 3 and 4). Isothermal sorption tests under balanced moisture conditions were performed with reference to standard GB/T 19 560-2008 using an IS-300 type isothermal adsorption instrument, and the test temperature was 30 °C. The adsorbent was methane gas with a purity of 99.99%.

2.2. Data processing methods

Coal is an object whose porosity, permeability, and other physical properties all have fractal characteristics. Many scholars have revealed the complexity of coal and rock components, and the severity of the coal
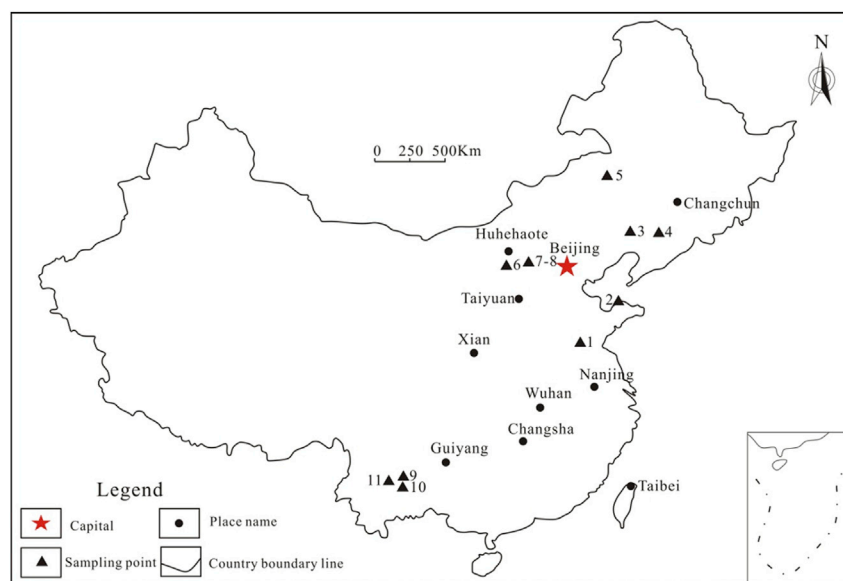

Fig. 1. Coal samples from 11 coal mines in China.
1. Taozhuang coal mine of Zaozhuang 2. Beizao coal mine of Longkou 3. Wulong coal mine of Fuxin 4. Laohutai coal mine of Fushun 5. Huolinhe open-pit mine 6. Heidaigou open-pit mine of Zhungeer 7. Tashan coal mine of Datong 8. Yungang coal mine of Datong 9. Xianfeng open-pit mine of Xundian 10. Kebao open-pit mine of Yiliang 11. Yipinglang coal mine of Lufeng.

Table 1
Output information of coal sample.

Coal sample number	Sampling sites	Lithotype of coal	Sedimentary characteristics	Stratigraphic age	Coal bearing stratum
1–1	Xianfeng open-pit mine of Xundian	detrital coal	river facies and lake facies	N	Xiaolong formation
1–2	Xianfeng open-pit mine of Xundian	xylitic coal			
2–1	Beizao coal mine of Longkou	xylitic coal	delta facies and lacustrine facies	E	Lijiaya formation
3–1	Kebao open-pit mine of Yiliang	mineral rich coal	lacustrine sedimentary system	N	Xiaolongtan formation
4–1	Huolinhe open-pit mine	xylitic coal	delta facies and lacustrine facies	J_3-K_1	Huolinhe formation
5–1	Laohutai coal mine of Fushun	bright coal	littoral-shallow lacustrine facies.	E	Guchengzi formation
6–1	Wulong coal mine of Fuxin	semi-bright coal	fan delta facies and fluvial facies	K_1	Fuxin formation
7–1	Heidaigou open-pit mine of Zhungeer	semi-bright coal	river delta facies	C_2-P_1	Taiyuan formation
7–2	Heidaigou open-pit mine of Zhungeer	semi-dull coal			
8–1	Yungang coal mine of Datong	dull coal	meandering facies	J_2	Datong formation
9–1	Tashan coal mine of Datong	dull coal	braided river facies	P_1	Shanxi formation
10–1	Yipinglang coal mine of Lufeng	semi-bright coal	delta sedimentary facies	T_3	Ganhaizi formation
11–1	Taozhuang coal mine of Zaozhuang	semi-dull coal	Sea-land interaction sedimentary facies	C_2-P_1	Taiyuan formation

Table 2
The basic information of coal sample.

Coal sample number	Industry analysis and $R_{o,max}$ test				Maceral with mineral matter/%			
	M_{ad} /%	A_d /%	V_{daf} /%	$R_{o,max}$ /%	Vitrinite (huminite) /%	Inertinite/%	Exinite/%	Mineral matter %
1–1	29.22	1.81	51.57	0.25	66.33	10.00	4.00	19.67
1–2	33.04	0.67	45.75	0.22	88.33	0.00	0.33	11.33
2–1	25.01	8.69	45.52	0.37	78.67	6.67	2.33	12.33
3–1	30.72	51.33	60.29	0.26	19.67	0.00	0.33	80.00
4–1	30.89	15.83	47.26	0.33	68.00	6.67	0.00	25.33
5–1	3.79	6.96	43.95	0.64	93.00	0.00	0.20	6.80
6–1	5.42	8.41	40.49	0.63	85.00	1.33	1.33	12.33
7–1	8.7	6.86	37.23	0.6	50.00	35.00	2.00	13.00
7–2	6.44	15.28	36.01	0.62	25.67	57.00	2.00	15.33
8–1	3.9	6.72	28.98	0.86	52.33	30.67	2.67	14.33
9–1	1.6	30.53	28.38	0.87	30.00	53.67	2.67	13.67
10–1	1.54	15.84	30.53	0.98	71.00	21.00	2.00	6.00
11–1	0.72	9.87	32.71	0.85	63.00	29.00	0.00	8.00

structure damage from the point of view of pore fractal law to study the complexity of pore structure and quantitatively characterize the percolation capacity (Cai et al., 2011; Zhang et al., 2014). The relation between pore radius and experimental pressure can be obtained as follows according to the mercury injection principle (Jiang et al., 2010).

$$r = \frac{106.633}{p} \tag{1}$$

According to the fractal definition, when a cylinder with a height of L and a radius of R is used to measure the pore volume of coal (V_m), V_m is related to D as follows:

$$V_m = C \pi r^{2-D} L \tag{2}$$

$$\log_{10}(V_m) = (D-2)\log_{10}\left(\frac{p}{106.633}\right) + \log_{10}(C\pi L) \tag{3}$$

$$D = K + 2 \tag{4}$$

Note: r is the pore radius, in nm; p is the experimental pressure, in psi; C is the proportionality constant; K is the slope of V_m and $\log_{10}\left(\frac{p}{106.633}\right)$; and D is the fractal dimension.

The equivalent desorption rate (M), equivalent desorption curvature

Table 3
The distribution of pore volume.

Coal sample number	Pore volume (cm³/g)					Pore volume ratio/%				Porosity/%
	V_1	V_2	V_3	V_4	V_t	V_1	V_2	V_3	V_4	
1–1	0.0256	0.0151	0.0327	0.0295	0.1029	24.88	14.67	31.78	28.67	11.82
1–2	0.0189	0.0130	0.0357	0.0315	0.0991	19.07	13.12	36.02	31.79	11.34
2–1	0.0272	0.0031	0.0151	0.0372	0.0826	32.93	3.75	18.28	45.04	9.62
3–1	0.0157	0.0098	0.0974	0.0261	0.1490	10.54	6.58	65.37	17.52	20.23
4–1	0.0249	0.0126	0.0695	0.0420	0.1490	16.71	8.46	46.64	28.19	16.42
5–1	0.0044	0.0015	0.0104	0.0195	0.0358	12.29	4.19	29.05	54.47	4.12
6–1	0.0090	0.0029	0.0100	0.0274	0.0493	18.26	5.88	20.28	55.58	6.03
7–1	0.0182	0.0299	0.0287	0.0509	0.1277	14.25	23.41	22.47	39.86	13.57
7–2	0.0058	0.0025	0.0184	0.0387	0.0654	8.87	3.82	28.13	59.17	8.25
8–1	0.0060	0.0137	0.0216	0.0246	0.0659	9.10	20.79	32.78	37.33	7.74
9–1	0.0038	0.0010	0.0064	0.0147	0.0259	14.67	3.86	24.71	56.76	3.39
10–1	0.0124	0.0018	0.0067	0.0143	0.0352	35.23	5.11	19.03	40.63	4.76
11–1	0.0051	0.0016	0.0083	0.0153	0.0303	16.83	5.28	27.39	50.50	3.96

Note: V_1, macropore volume (>1000 nm); V_2, mesopore volume (100–1000 nm), V_3, transition pore volume (10–100 nm), V_4, micropore volume (<10 nm); V_t, total volume.

Table 4
The distribution of pore specific surface area.

Coal sample number	Pore specific surface area (cm²/g)					Pore specific surface area ratio/%				Average pore diameter/nm
	S_1	S_2	S_3	S_4	S_t	S_1	S_2	S_3	S_4	
1–1	0.003	0.348	4.861	24.448	29.660	0.01	1.17	16.39	82.43	14.1
1–2	0.004	0.234	6.330	25.415	31.983	0.01	0.73	19.79	79.46	12.8
2–1	0.004	0.051	3.036	31.210	34.301	0.01	0.15	8.85	90.99	9.8
3–1	0.005	0.190	19.557	17.826	37.578	0.01	0.51	52.04	47.44	16.0
4–1	0.007	0.249	11.453	32.915	44.624	0.02	0.56	25.67	73.76	13.6
5–1	0.001	0.030	2.107	15.950	18.088	0.01	0.17	11.65	88.18	8.1
6–1	0.003	0.043	2.112	23.287	25.445	0.01	0.17	8.30	91.52	7.9
7–1	0.023	0.375	5.474	39.168	45.040	0.05	0.83	12.15	86.96	11.5
7–2	0.001	0.044	4.132	29.801	33.978	0.00	0.13	12.16	87.71	7.8
8–1	0.004	0.273	3.450	20.346	24.073	0.02	1.13	14.33	84.52	11.0
9–1	0.000	0.016	1.329	12.236	13.581	0.00	0.12	9.79	90.10	7.9
10–1	0.004	0.027	1.422	12.054	13.507	0.03	0.20	10.53	89.24	11.7
11–1	0.000	0.030	1.671	12.267	13.968	0.00	0.21	11.96	87.82	8.9

Note: S_1, macropore specific surface area (>1000 nm); S_2, mesopore specific surface area (100–1000 nm), S_3, transition pore specific surface area (10–100 nm), S_4, micropore specific surface area (<10 nm); S_t, total specific surface area.

(K), and the slope of the curvature (S) are calculated as follows:

$$M = \frac{V_L P_L}{(P + P_L)^2} \quad (5)$$

$$K = \frac{\frac{6 V_L P_L}{(P+P_L)^4}}{\left\{ 1 + \left[\frac{2 V_L P_L}{(P+P_L)^3} \right]^2 \right\}^{1.5}} \quad (6)$$

$$S = \frac{-24 V_L P_L}{(P + P_L)^5} \times \left\{ 1 + \left[\frac{2 V_L P_L}{P + P_L} \right]^2 \right\}^{-1.5} + \frac{216 (V_L P_L)^3}{(P + P_L)^{11}}$$
$$\times \left\{ 1 + \left[\frac{2 V_L P_L}{(P + P_L)^3} \right]^2 \right\}^{-2.5} \quad (7)$$

Note: M is the CBM desorption under unit pressure drop conditions, measured in cm³/g·Mpa; V_L is the Langmuir volume, in cm³/g; P_L is the Langmuir pressure, in MPa; K is the equivalent desorption curvature; and S is the slope of the curvature.
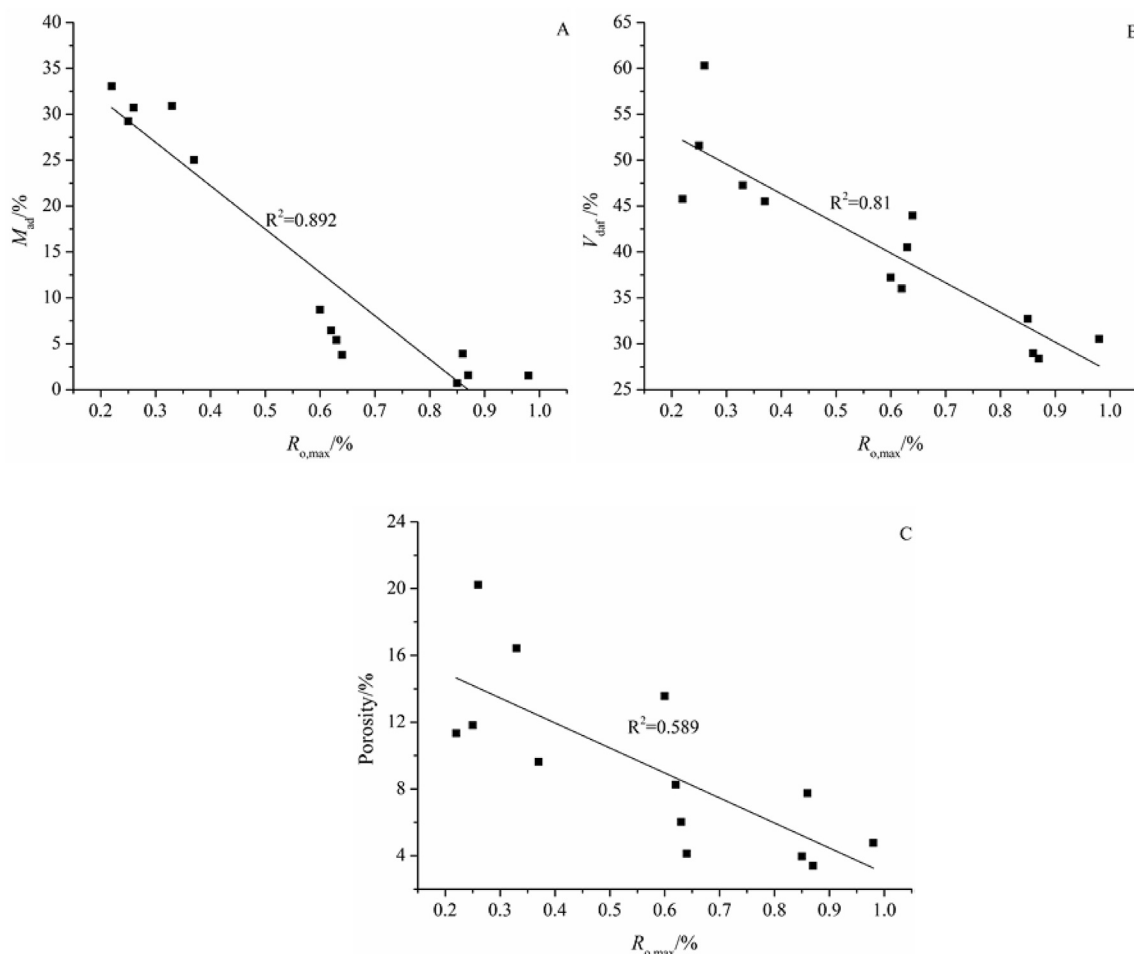

Fig. 2. The relationship between M_{ad}, V_{daf}, porosity and R_o.
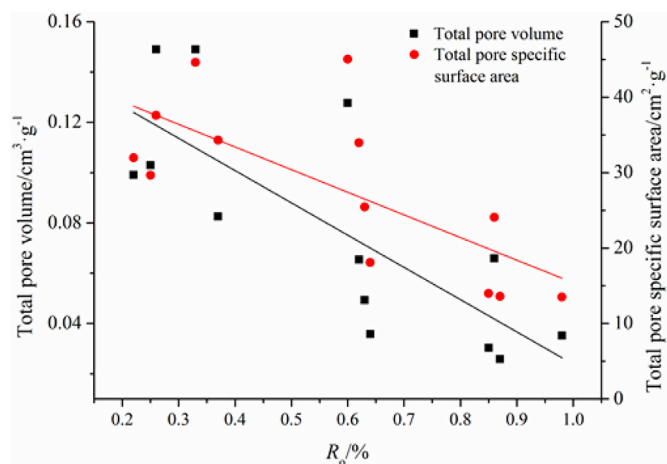
Fig. 3. The relationship between total pore volume, total pore specific surface area and R_o.

3. Results and discussion

3.1. Basic properties of the coal sample

The $R_{o,max}$ is between 0.22% and 0.98%, and the coal rank ranges from lignite to long-flame coal, to gas coal. The macerals of different rank coals indicate that the content of vitrinite (huminite) is between 19.67% and 93%, with an average of 60.84%; the content of inertinite is between 0% and 53.67%, with an average of 18.31%; the content of exinite is between 0% and 4%, with an average of 1.53%; and the content of the mineral is between 6% and 80%, with an average of 18.31%. The moisture content of lignite is the highest because there are many polar functional groups, which show strong hydrophilicity when the degree of coal metamorphism is low. The coal structure is loose and porous, and the pore is dominated by large pores, which provides favorable conditions for the occurrence of moisture. With the increasing degree of coalification, the lateral chain alkyl and functional groups fall off, and the order of the molecular structure of the coal increases gradually (Fig. 2A). At the same time, the gradual improvement of the coalification degree will also lead to the reduction of the volatile components of the coal and rock components (Fig. 2B). During the burial process, the structure of coal becomes compact and the moisture content decreases (Fig. 2A and C). The ash content is mainly affected by the composition of the material, such as No.3-1 coal, the mineral composition, and ash yield are highest (Table 2).

The mineral composition of the coal sample is dominated by clay minerals, followed by pyrite. The pyrite of lignite is higher, the average accounted for 48.56% of the total mineral content, and the clay mineral in long-flame coal is the highest, where the average accounted for 84.22% of the to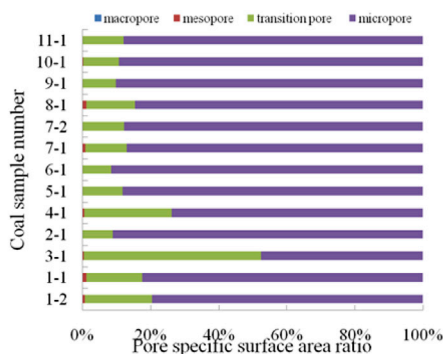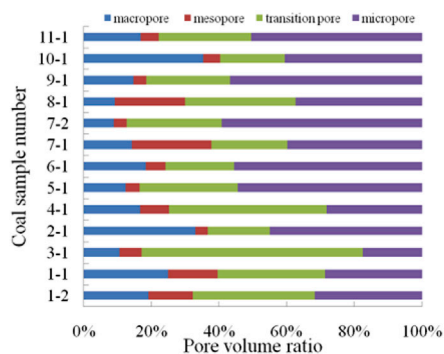tal mineral content, and the content of pyrite and clay mineral in gas coal is somewhere in between. The minerals in the coal were distributed in bands, or present as massive and lenticular in the macerals, and they were also dispersed in the macerals or intermixed with detrital fragments of macerals, mainly in later generations.

3.2. Pore distribution characteristics

The mercury intrusion test showed that the total pore volume distribution of different rank coals ranged from 0.0259 cm^3/g to 0.149 cm^3/g, with an average of 0.0783 cm^3/g, and the total pore specific surface area is distributed from 13.507 cm^2/g to 45.040 cm^2/g, with an average of 28.14 cm^2/g, and the total pore volume and the total pore specific surface are showed a decreasing trend with the increased coal rank (Fig. 3). The distribution of specific surface area and pore volume of different rank coals are the same, and both are mainly based on micropores and transition pores (Fig. 4). The pore volume of different pore sizes overall decreases with the increase of coal rank. Among them, the reduction extent of the macro-pore is the largest, and the other pores show that attenuation decreases and stabilizes gradually as $R_{o,max}$ is greater than 0.6% (Fig. 5). The average pore size of the sample is between 7.8 nm and 16 nm, with an average of 10.85 nm. The average pore size of the lignite is the largest, indicating that the compaction of coal and the adsorption and filling effect of a large number of associated strong adhesion and fluorescent asphaltene due to the disappearance or reduction of macromolecular oxygen-containing functional groups and alkyl side chains of coal results in the decrease of pore size in coal with the increase of coal rank. Among them, the macro-pore contribution rate is the largest, and the pore size distribution in coal is gradually uniform (Jian et al., 2015).

3.3. Pore fractal characteristics

The pore structure of coal reservoirs is extremely complex. When a fractal study is performed, the fractal characteristics of different scales should be studied according to the pore size range and actual distribution to reflect the real situation of pore structure in a coal reservoir (Zhou et al., 2017b). There are two obvious turning points in $log_{10}(V_m)$ and $log_{10}(p/106.633)$, and the corresponding aperture of the turning point is 6,000 nm and 100 nm, respectively. The linear relationship has three distinct phases, and there are three different pore structures corresponding to each phase. That is, the adsorption-diffusion pore is between 3 nm and 100 nm, the secondary seepage pore is between 100 nm and 6,000 nm, and the primary seepage pore is larger than 6,000 nm. The R^2 of all are greater than 0.9, indicating that the pores of the sample have good fractal characteristics in the proper pore size range, where the corresponding pore fractal dimensions are D_3, D_2, and D_1 (Fig. 6).

The fractal dimension under different pore sizes of different rank coals is between 2 and 3 (Table 5). Among them, the average fractal dimension of the primary seepage pore is the highest (2.6), followed by the adsorption-diffusion pore (2.39), and the secondary seepage pore is
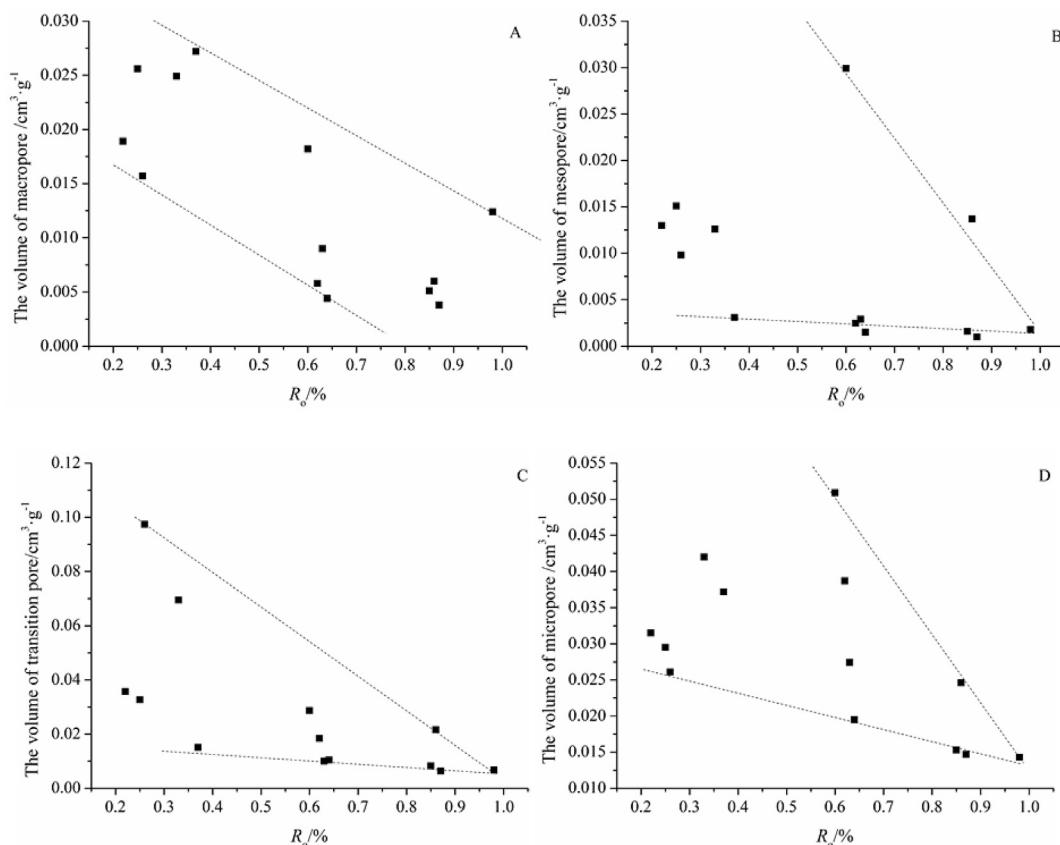

Fig. 4. Pore volume and pore specific surface area distribution for different pores.

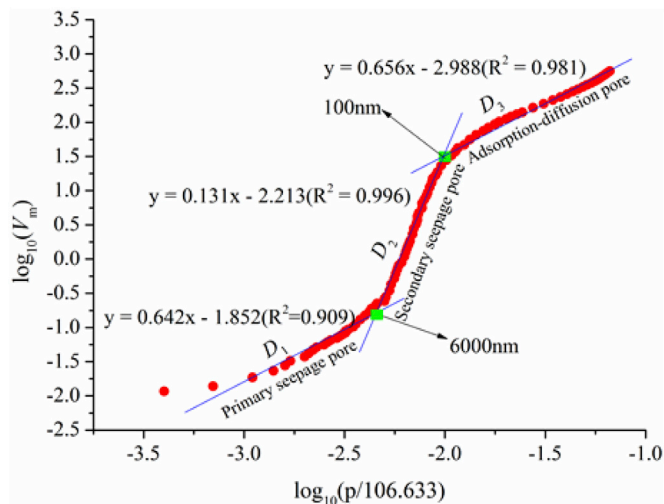Fig. 5. The relationship between pore volume of each pore and R_o.

Fig. 6. The relationship between $\log_{10}(V_m)$ and $\log_{10}(p/106.633)$ of No.7-2 coal.

the lowest (2.15). The relationship between fractal dimension and metamorphism degree in different pore sizes is different. There is a negative correlation between D_1 and $R_{o,max}$, but there is no correlation between D_2 and $R_{o,max}$, and the fractal dimension is mainly concentrated below 2.2. Furthermore, D_3 shows a parabolic change with the degree of metamorphism, and the highest point is around 0.5%–0.6% of $R_{o,max}$, but the correlation is smaller (Fig. 7A and B). The above characteristics show that the effect of coal metamorphism on porosity is mainly reflected in the control of the primary seepage pore structure. The reason is that the diagenesis of sedimentary compaction and dehydration leads to the

seepage pore is gradually compressed and averaged in the early stage of coal metamorphism, and the early metamorphism mainly results in the random distribution and complexity of the adsorption-diffusion pore. Therefore, the seepage pore structure (>6,000 nm) tends to be simple with the increase of R_o (Chen, 2001).

There is a positive correlation between D_3 and the coal metamorphism degree under R_o, which is lower than 0.6 (Fig. 7C). The main reason is that the asphalt-filling effect makes the pore structure of both the transition pore and micro-pore complex during the early diagenetic stage. With the increase of metamorphic degree, the pore produced by thermal hydrocarbon generation makes the pore between 10 nm and 100 nm increase, and the asphalt-filling effect is less than the early diagenetic stage. Therefore, the structure of transition pore and micro-pore improved later (Jian et al., 2015). In addition, D_3 was mainly affected by the ash yield and the content of vitrinite (huminite) which had a positive correlation with the former, but negatively correlated with the latter (Fig. 7D). The main reason is that the ash yield, as a derivative of the minerals in the coal, can reflect certain mineral information. The filling of minerals often results in an increase in pore roughness and an increase in heterogeneity. From the above analysis, it can be seen that the minerals in the samples are mainly clay minerals and are distributed in the transition pore and micro-pore in different states, so the fractal dimension is enhanced. Vitrinite (huminite) has the highest proportion of micro-pore in the macerals (Lamberson and Bustin, 1993; Faiz and Hutton, 1995; Clarkson and Bustin, 1999; Bustin and Clarkson, 1998; Crosdale et al., 1998; Laxminarayana and Crosdale, 2002), and the pores of different rank coal seams are mainly micro-pores and transition pores, so it plays an important role in controlling the pore characteristics of different rank coals.

Previous studies generally believe that the larger the pore fractal dimension, the greater the pore roughness, while the worse the pore connectivity, the stronger the heterogeneity and the more detrimental to

Table 5
Pore fractal dimension.

Coal sample number	D_1	Fitting formula	D_2	Fitting formula	D_3	Fitting formula
1–1	2.767	y = 0.767x - 0.988	2.113	y = 0.113x - 1.577	2.237	y = 0.237x - 1.643
1–2	2.563	y = 0.563x - 1.294	2.152	y = 0.152x - 1.673	2.317	y = 0.317x - 1.861
2–1	2.836	y = 0.836x - 0.932	2.041	y = 0.041x - 1.545	2.297	y = 0.297x - 1.943
3–1	2.613	y = 0.613x - 1.444	2.163	y = 0.163x - 1.803	2.565	y = 0.565x - 2.270
4–1	2.645	y = 0.645x - 1.155	2.129	y = 0.129x - 1.584	2.374	y = 0.374x - 1.817
5–1	2.411	y = 0.411x - 2.004	2.083	y = 0.083x - 2.291	2.523	y = 0.523x - 2.9
6–1	2.722	y = 0.722x - 1.637	2.111	y = 0.111x - 2.032	2.428	y = 0.428x - 2.541
7–1	2.711	y = 0.711x - 1.493	2.476	y = 0.476x - 1.810	2.301	y = 0.301x - 1.742
7–2	2.642	y = 0.642x - 1.852	2.131	y = 0.131x - 2.213	2.656	y = 0.656x - 2.988
8–1	2.649	y = 0.649x - 1.915	2.374	y = 0.374x - 2.227	2.318	y = 0.318x - 2.071
9–1	2.433	y = 0.433x - 2.049	2.071	y = 0.071x - 2.330	2.483	y = 0.483x - 2.947
10–1	2.341	y = 0.341x - 1.584	2.062	y = 0.062x - 1.804	2.239	y = 0.239x - 2.103
11–1	2.476	y = 0.476x - 1.952	2.094	y = 0.094x - 2.231	2.434	y = 0.434x - 2.734

Note: D_1, the fractal dimensions of the primary seepage pore; D_2, the fractal dimensions of the secondary seepage pore; D_3, the fractal dimensions of the adsorption-diffusion pore.

the seepage flow (Zhao et al., 2014). This is contrary to the conclusions of this study because the influence of pore fractal dimension on the seepage has not removed the effect of the adsorption pore (<100 nm) in the previous studies. Based on the theory of porosity hysteresis loops, the greater the volume difference between the mercury injection curve and the withdrawal curve, the higher the proportion of open pore, the better the pore connectivity, and the more conducive to seepage (Fu et al., 2015). The mercury curve of the sample is divided into three types. Type I (such as No.3-1 coal) is that the mercury injection curve tends to parallel with the withdrawal curve, and the volume difference between them increases slowly with the decrease of pressure, when the aperture is larger than 100 nm, indicating that the number of open holes is limited. TypeII(such as No.7-1 coal) the volume difference between the mercury injection curve and the withdrawal curve is bigger and bigger with the decrease of pressure, when the aperture is larger than 1000 nm, the mercury injection curve tends to parallel with the withdrawal curve, and the increase of opening hole tends to be slow, so the ratio of open pores in seepage poles of TypeIIis higher than that of Type I. Type III (such as No.10-1 coal) is that the mercury injection curve come closest to the withdrawal curve, and hysteresis loops are not apparent at all pore sizes, indicating that the pores are dominated by semi-closed pores, which is unfavorable to seepage (Fig. 8). Therefore, the seepage capacity from high to low is TypeII, Type I and TypeIII, and the fractal dimension of the seepage pore (D_1, D_2) show the same rules, indicating that the larger the fractal dimension of the pore is, the more conducive to the development of the open hole and the more favorable to the seepage of the coal reservoir. The fractal dimension (D_1) is the key factor to determine the permeability of the coal reservoir because the fractal dimension (D_2) of the coal sample has little difference. Combined with the above analysis,
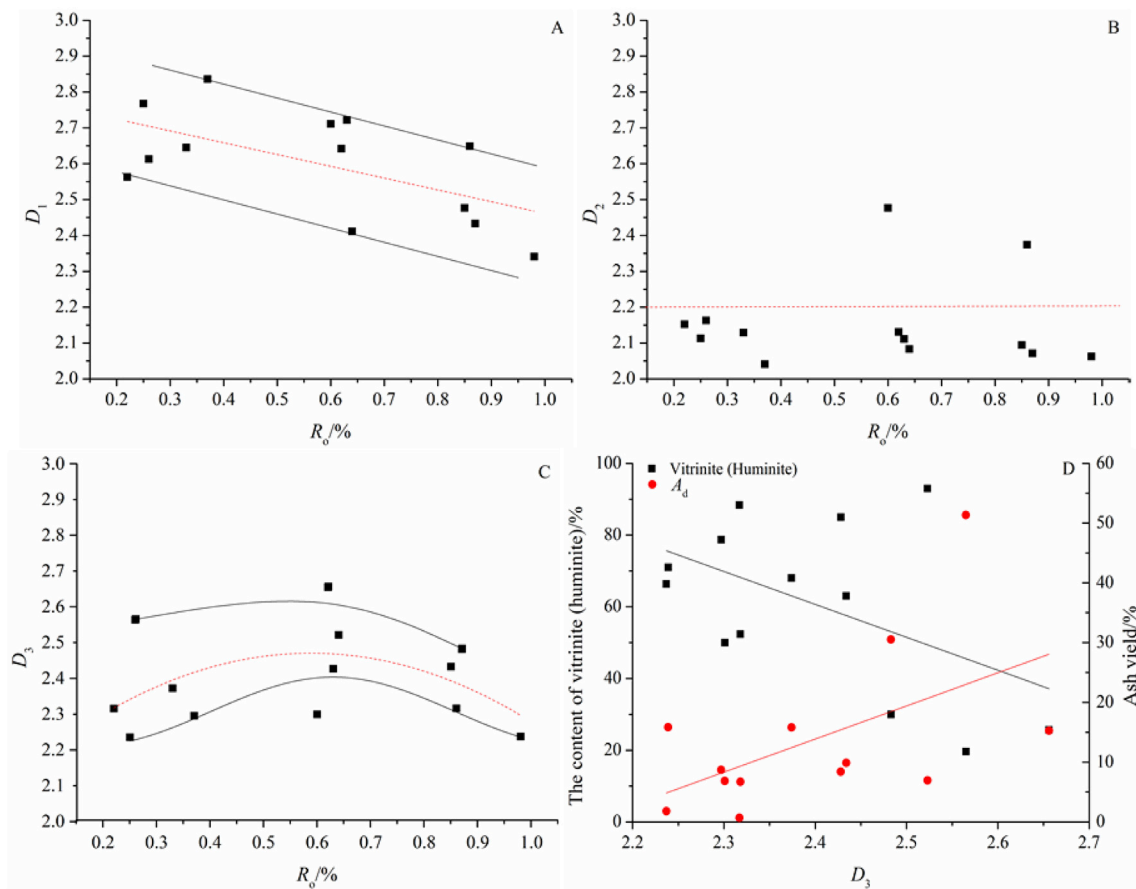

Fig. 7. Fractal dimension of different pores and its relation with R_o, the content of vitrinite (huminite), and ash yield.
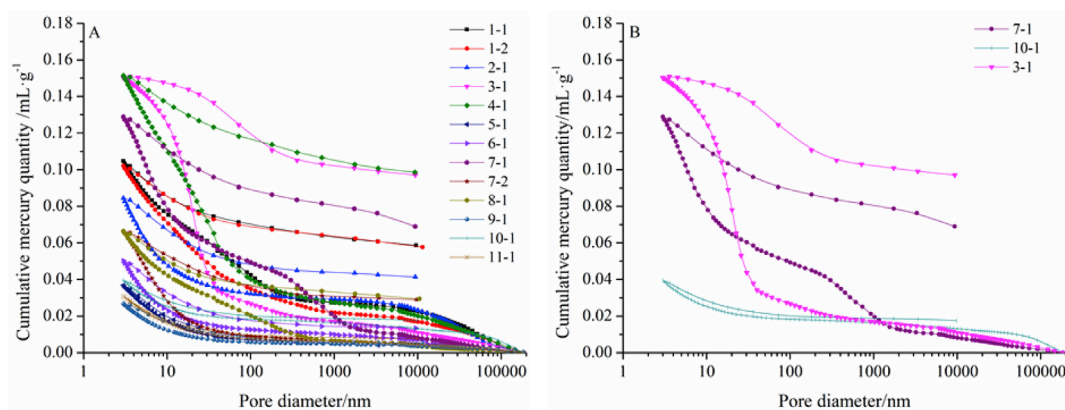
Fig. 8. Mercury injection and withdrawal curve of different rank coals.

the average fractal dimension of seepage holes (D_1) form high to low is as follow: lignite (2.68), long flame coal (2.62), gas coal (2.47), indicating that the open pore of lignite is more and the distribution of pore throat is relatively concentrated and relatively large, which is most favorable for the seepage of coalbed methane.

3.4. Adsorption characteristics

The Langmuir model of adsorption of the monomolecular layer is applied to fit the experimental results of the isothermal adsorption under equilibrium moisture (Gray, 1987; Mavor et al., 1990). The results show that the V_L of low- and medium-rank coals is between $4.68\,m^3/t$ and $8.44\,m^3/t$, and P_L is between 2.28 and 3.09 (Table 6). The isothermal adsorption of coal is mainly affected by the pore structure, the composition, and the chemical structure of the coal (Yee et al., 1993; Allardice et al., 2003; Crosdale et al, 2008; Wang et al., 2011).

Furthermore, V_L has a significant positive correlation with the degree of coal metamorphism (Fig. 9A). The essence of the evolution of coal rank from low to high is attributed to the continuous evolution of coal's molecular structure with coalification degree. It shows that the molecular structure of coal is the basic factor to control its adsorption characteristics for low- and medium-rank coals. It is precisely because of the existence of the above relationship, the degree of coal metamorphism can be judged by V_L In the following discussion. The influence of the composition of coal on the adsorption is manifested in no correlation between the content of vitrinite (huminite) and the maximum adsorption capacity in lignite and long-flame coal stage, they only show the effect on the maximum adsorption capacity in the gas coal stage. The maximum adsorption capacity was positively correlated with the content of inertinite, but no correlation existed with the content of exinite, indicating that the effect of the macerals on the adsorption of low- and medium-rank coals is weak (Fig. 9B). There was a negative correlation between the maximum adsorption capacity and moisture content, and a slight positive correlation with the ash content (Fig. 9C). The reason is that the moisture reduces the adsorption capacity; on the other hand, it blocks the adsorption channel of the coal with the increase of moisture content (Guo et al., 2015). The ash is a comprehensive reflection of the minerals. The

mineral types of this sample are mostly clay minerals, so it is beneficial to the adsorption of methane.

The influence of the pore structure on adsorption showed that the maximum adsorption capacity was negatively correlated with D_1. The volume of the seepage pore and adsorption pore increase simultaneously with the increase of D_1, but the former growth rate is higher than the latter (Fig. 10), indicating that the lower the adsorption pore content, the less favorable it is for methane adsorption. According to the above analysis, the D_2 of different samples have little difference, so it has little influence on adsorbability (Fig. 9D). There was a negative correlation between the maximum adsorption capacity and D_3 in the long-flame coal and gas coal stage (Fig. 9E), indicating that the pore fractal dimension of the adsorption pore (pore diameter is less than100 nm) is smaller, the simpler the pore structure, and the smoother the surface is more conducive to adsorption. The D_3 of the long-flame coal (average 2.477) is greater than that of gas coal; thus, the maximum adsorption capacity of gas coal is higher than that of long-flame coal, and the results coincide with the isothermal adsorption. The maximum adsorption has no or a weaker relation with D_3 in the lignite stage (Fig. 9E). The main reason is that the oxygen functional group in lignite is the highest, and it is easy to adsorb moisture. Even if the specific surface area is the largest, the effective specific surface area is small, so the adsorption of methane is also the lowest (Gan et al., 1972).

In summary, the adsorption of low- and medium-rank coal is a step-by-step process under the control of coal metamorphism, which lignite mainly depends on the moisture level, long-flame coal-gas coal mainly depends on the adsorption-diffusion hole (<100 nm) pore structure.

3.5. Desorption characteristics and their implications for coalbed methane development

Under the conditions of a saturated coal sample, which does not consider the impact of gas saturation, the characteristics of the pressure decline and desorption are described using the numerical method proposed by Zhang et al. (2013), where the desorption stage of coalbed methane is characterized by an equivalent desorption rate and its curve characteristics. The results show that the effective desorption rate of

Table 6
Isothermal adsorption parameter of coal sample.

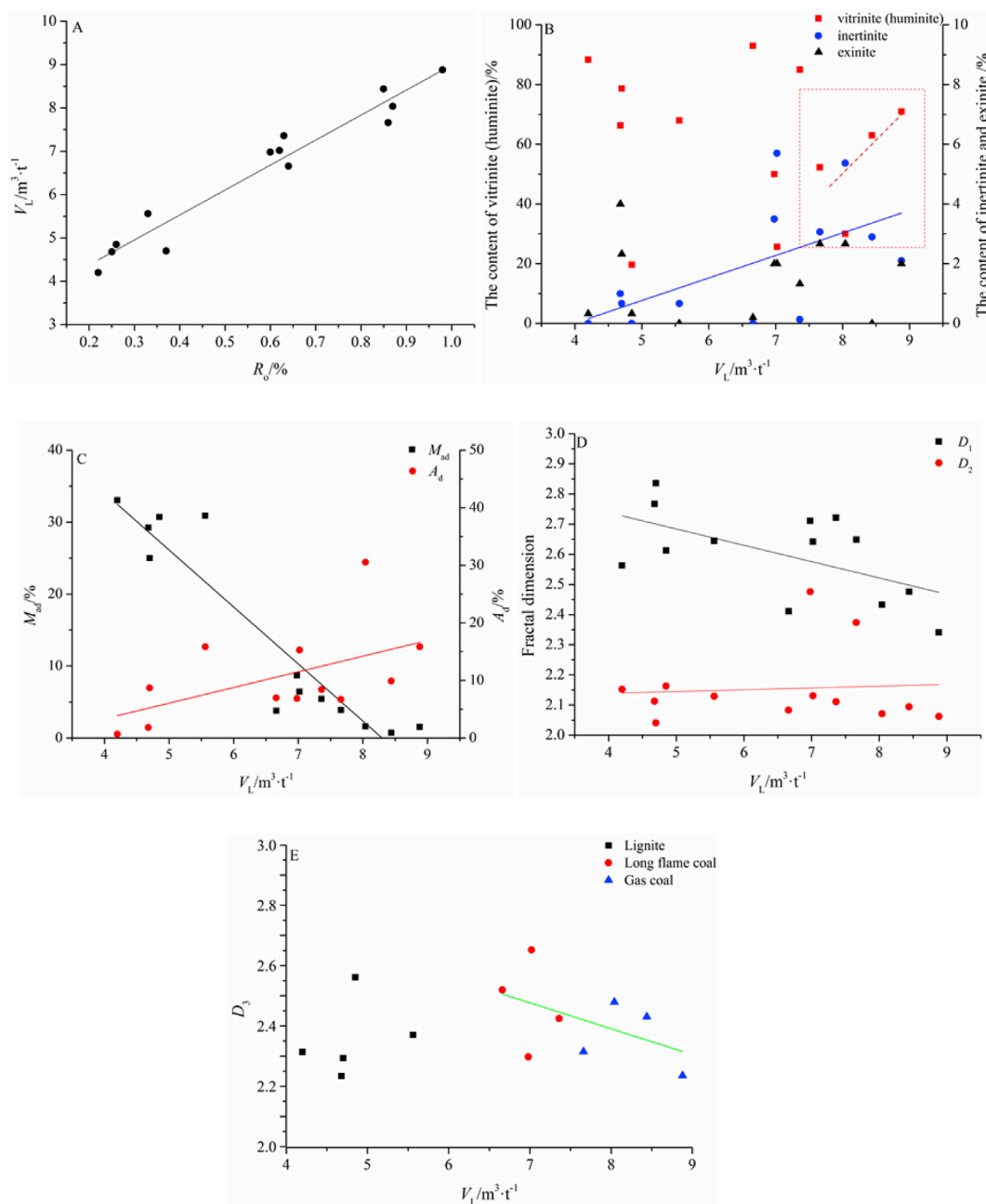| Coal sample number	V_L (m³/t)	P_L (MPa)	Equilibrium moisture/%	Coal sample number	V_L (m³/t)	P_L (MPa)	Equilibrium moisture/(%)
1–1	4.68	2.80	4.65	7–1	6.98	3.09	3.68
1–2	4.20	2.45	4.12	7–2	7.02	3.17	3.62
2–1	4.70	2.53	3.69	8–1	7.66	2.72	3.05
3–1	4.85	2.78	4.28	9–1	8.04	2.28	3.25
4–1	5.56	2.45	3.68	10–1	8.88	2.39	3.27
5–1	6.66	2.34	3.12	11–1	8.44	2.44	3.62
6–1	7.36	2.87	3.16				

Fig. 9. The relationship between V_L and maceral, ash, moisture, and D_3.

different rank coals increases gradually with decreasing pressure. The desorption rate is approximately zero in the initial stage of the pressure drop. As the pressure continues to decrease, the equivalent desorption rate experiences a slow increase to a rapid increase process, but the maximum equivalent desorption rate increases with the increase of the coal rank (Fig. 11A), and the pressure corresponding to the maximum equivalent desorption curvature extreme point increases with the increasing coal rank (Fig. 11B). According to the four desorption stages which are divided by starting pressure, transition pressure, and sensitive pressure, the sensitive desorption stage does not exist in the lignite to long-flame coal stage (Fig. 11C).

The model of Zhang et al. (2013) is based on the premise that adsorption and desorption is reversible, but coal adsorption and desorption is a non-reversible process under actual conditions (Menon, 1968; Cui et al., 2004; Wang et al., 2014), indicating that some gas remains in the pore under natural desorption conditions. This extreme

pressure is similar to the depletion pressure in CBM drainage, which is the maximum curvature (Fig. 11C). Through the above analysis, although the sensitive desorption stage exists in the gas coal, the sensitive pressure is close to 0Mpa, indicating that this process is short compared to the other three desorption stages. Based on this, the desorption stage of low- and medium-rank coals is subdivided into zero desorption, transient desorption, mass desorption, and residual desorption, according to the starting pressure, the transition pressure, and the depletion pressure (Fig. 11B and C) (Table 7). The coal seam began to slow desorption as the pressure drops to the critical desorption pressure. When the transition pressure is obtained, the curvature slope reaches the maximum, indicating a transition stage from slow desorption to large desorption. The curvature reaches its maximum as the depletion pressure is reached, but the absolute value of the curvature change rate is lower in this process. The reason is that the closer to the depletion pressure, the more difficult to reduce the reservoir pressure and the more obvious the desorption
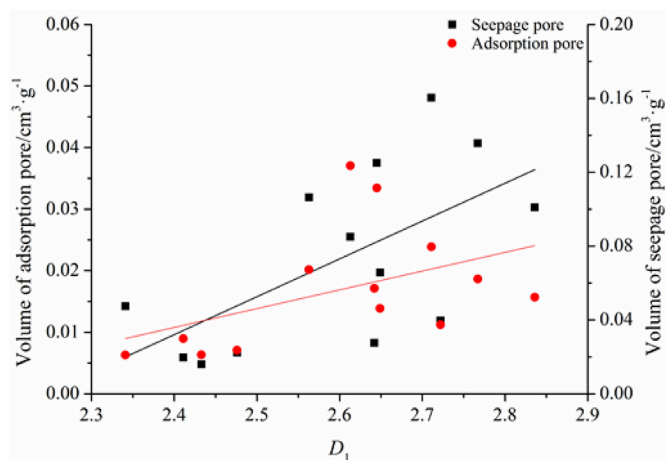
Fig. 10. The relationship between D_1 and volume of adsorption pore and seepage pore.

Table 7
Key pressure points of different rank coals.

Coal sample number	Starting pressure/Mpa	Transition pressure/Mpa	Depletion pressure/Mpa	Sensitive pressure/Mpa
1–1	5.1	1	0.3	0
1–2	5	1.1	0.4	0
2–1	5.2	1.2	0.5	0
3–1	5.1	1.1	0.3	0
4–1	5.5	1.4	0.7	0
5–1	5.8	1.7	0.9	0
6–1	5.8	1.6	0.7	0
7–1	5.5	1.5	0.6	0
7–2	5.5	1.5	0.5	0
8–1	5.9	1.8	0.9	0
9–1	6.1	2	1.2	0.3
10–1	6.3	2.1	1.2	0.3
11–1	6.2	2	1.1	0.2

hysteresis effect and the gas production is lower. The desorption rate of the coal reservoir should be maximum as the depletion pressure is reached, but the equivalent desorption rate still increases from the depletion pressure to 0Mpa, which is contrary to the conventional CBM drainage process. The main reason is that if the coalbed methane is completely desorbed, the residual gas in the coal reservoir cannot be desorbed even if the pressure is reduced to 0Mpa.Therefore, only through the method of increasing the reservoir permeability, such as CO_2 injection and ultrasonic treatment, the coalbed methane can be completely desorbed.

The critical pressure point has a great influence on the coalbed methane productivity, so the control factors of different critical pressure points are particularly important. From the above analysis, we can see that the pore structure of the coal, the composition of the coal, and the influence of the chemical structure are key to control the adsorption of coal, and also the key factor to control desorption. The controlling effect of the chemical structure on the coal seam desorption is mainly manifested in that different critical pressure points increase with increased metamorphic degree (Fig. 12A). There is a negative correlation between the different critical pressure points and D_1, but there is no correlation with D_2 and D_3 (Fig. 12B). However, there is a negative correlation between different critical pressure points and moisture content, indicating that the pore structure of the seepage pore is more favorable to the seepage; the easier to combine the moisture in the coal reservoir and the more the oxygen-containing functional group combined with moisture, the lower the adsorbed gas content and the more difficult to produce the coalbed methane (Fig. 12C). Different critical pressure points were positively correlated with V_L, but negatively correlated with P_L,

indicating that the high adsorption gas content is beneficial to the early arrival of gas and stable production time, but is not conducive to sustained CBM step-down desorption of coalbed methane production, resulting in a declining stage appearing in advance (Fig. 12D and E).

4. Conclusions

There are three different pore structures in different rank coals. They are primary seepage pore, secondary seepage pore, and adsorption-diffusion pore, according to the pore diameter boundaries of 6,000 nm and 100 nm. The pore fractal dimension (D_1) is controlled by the degree of metamorphism, and D_3 is mainly affected by the ash yield, the content of vitrinite (huminite), and the degree of metamorphism.

The adsorption of low- and medium-rank coal is a step-by-step process under the control of coal metamorphism, which lignite mainly depends on the moisture level, and long-flame coal-gas coal mainly depends on the adsorption-diffusion hole (<100 nm) pore structure. The lower the fractal dimension of adsorption pore, the better the adsorption. The higher the fractal dimension of the seepage pore, the better the seepage.

The desorption stage of low- and medium-rank coals is subdivided into zero desorption, transient desorption, mass desorption, and residual desorption, according to the starting pressure, the transition pressure, and the depletion pressure. The different critical pressure points are mainly affected by the degree of coal metamorphism, the pore structure characteristics of the primary seepage pore, and the combined effects of moisture. The different critical pressure points relationship with V_L and P_L indicate that the high adsorption gas content is beneficial to the early arrival of gas and stable production time, but less favorable to the continuous depressurization and desorption of CBM, resulting in a decreases CBM production capacity ahead of time.
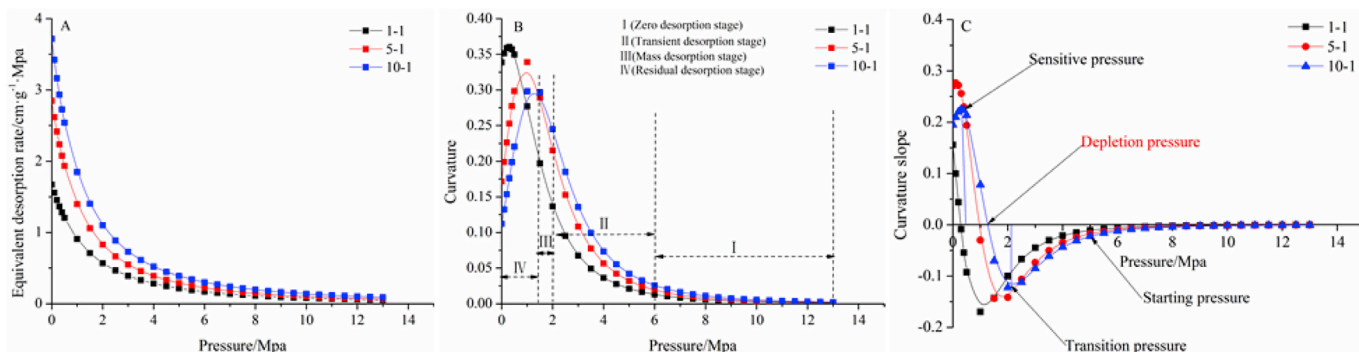

Fig. 11. The relationship between equivalent desorption rate, curvature, curvature slope, and pressure.
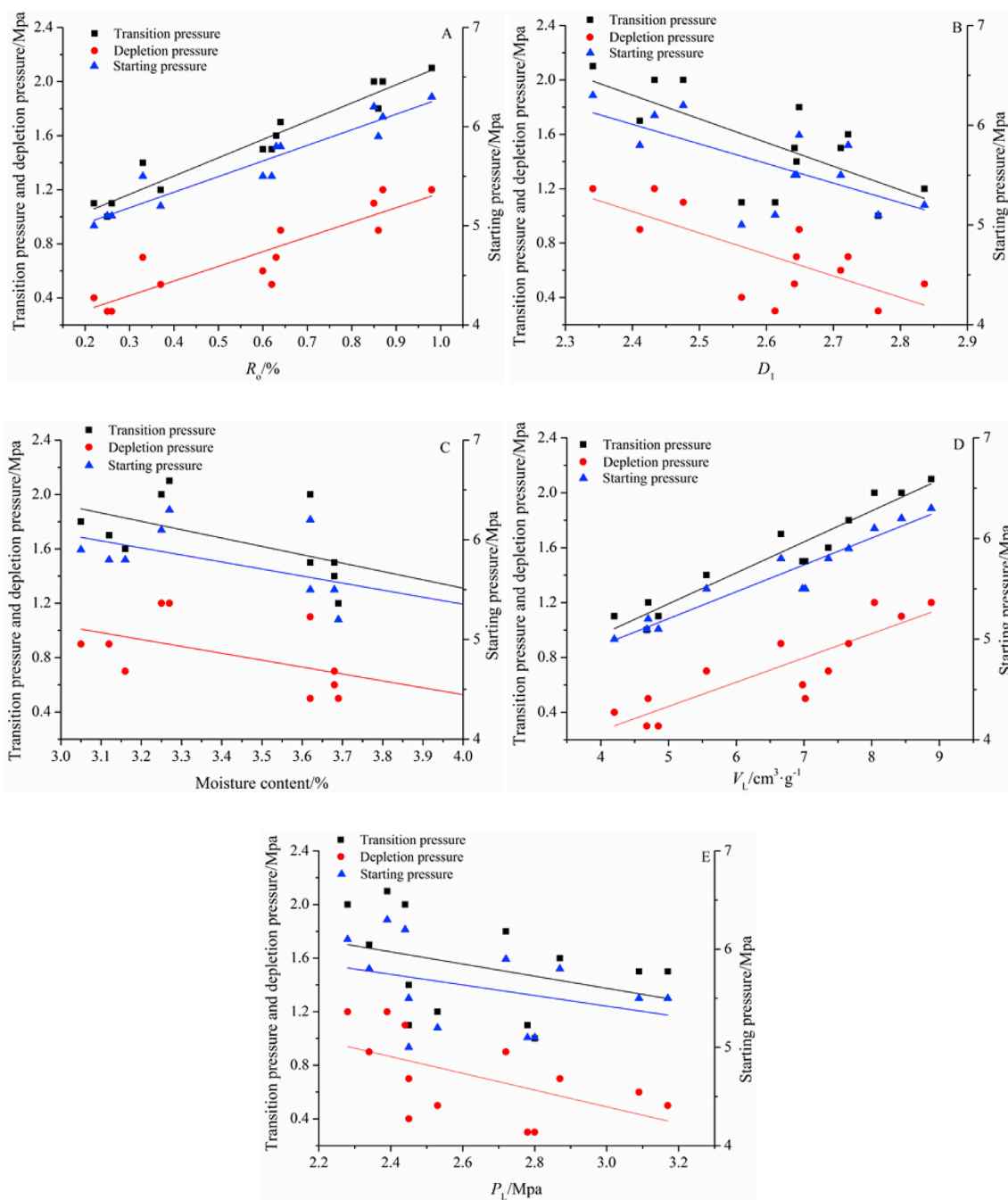
Fig. 12. The relationship between critical pressure and R_o, D_1, moisture content, P_L, and V_L.

Acknowledgments

References

Allardice, D.J., Clemow, L.M., Favas, G., Jackson, W.R., 2003. The characterisation of different forms of water in low rank coals and some hydrothermally dried products. Fuel 82 (6), 661–667.

Bustin, R.M., Clarkson, C.R., 1998. Geological controls on coalbed methane reservoir capacity and gas content. Int. J. Coal Geol. 38 (1), 3–26.

Cai, Y.D., Liu, D.M., Yao, Y.B., Li, J.Q., Liu, J.L., 2011. Fractal characteristics of coal pores based on classic geometry and thermodynamics models. Acta Geol. Sin. 85, 1150–1162.

Clarkson, C.R., Bustin, R.M., 1999. The effect of pore structure and gas pressure upon the transport properties of coal: a laboratory and modeling study. 1. Isotherms and pore volume distributions. Fuel 78 (11), 1333–1344.

Clarkson, C.R., Bustin, R.M., 2000. Binary gas adsorption/desorption isotherms: effect of moisture and coal composition upon carbon dioxide selectivity over methane. Int. J. Coal Geol. 42 (4), 241–271.

Crosdale, P.J., Beamish, B.B., Valix, M., 1998. Coalbed methane sorption related to coal composition. Int. J. Coal Geol. 35 (1), 147–158.

Crosdale, P.J., Moore, T.A., Mares, T.E., 2008. Influence of moisture content and temperature on methane adsorption isotherm analysis for coals from a low-rank, biogenically-sourced gas reservoir. Int. J. Coal Geol. 76 (1), 166–174.

Cui, X., Bustin, R.M., Dipple, G., 2004. Selective transport of CO_2, CH_4, and N_2 in coals: insights from modeling of experimental gas adsorption data. Fuel 83 (3), 293–303.

Chen, P., 2001. Characteristics, Classification and Utilization of Coal in China. Chemical Industry Press, Beijing, pp. 81–83 (In Chinese).

Deng, C., Tang, D., Liu, S., Xu, H., Tao, S., 2015. Characterization of mineral composition and its influence on microstructure and sorption capacity of coal. J. Nat. Gas Sci. Eng. 2015 (25), 46–57.

Faiz, M.M., Hutton, A.C., 1995. Geological controls on the distribution of CH_4 and CO_2 in coal seam gas of the Southern Coalfield, NSW, Australia. In: International Symposium-CUM-workshop on Management and Control of High Gas Emissions and Outbursts in Underground Coal Mines, Wollongong, NSW, Australia, pp. 375–383.

Fu, H., Tang, D., Xu, T., Xu, H., Tao, S., Li, S., Yin, Z.Y., Chen, B.L., Zhang, C., Wang, L.L., 2017. Characteristics of pore structure and fractal dimension of low-rank coal: a case study of Lower Jurassic Xishanyao coal in the southern Junggar Basin, NW China. Fuel 2017 (193), 254–264.

Fu, X.H., Jian, K., Ding, Y.M., Wang, K.X., 2015. Gas content Simulation of Three-phase State in Low Rank Coal Reservoir. Science press, Beijing (In Chinese).

Gan, H., Nandi, S.P., Walker, P.L., 1972. Nature of the porosity in American coals. Fuel 51 (4), 272–277.

Guo, H., Cheng, Y., Wang, L., Jin, K., 2015. Experimental study on the effect of moisture on low-rank coal adsorption characteristics. J. Nat. Gas Sci. Eng. 24, 245–251.

Gray, I., 1987. Reservoir engineering in coal seams: Part 1-The physical process of gas storage and movement in coal seams. SPE Reservoir Eng. 2 (01), 28–34.

Hodot, B.B., 1966. Outburst of Coal and Coalbed Gas (Chinese Translation). China Coal Industry Press, Beijing, pp. 18–33.

Hou, Q.L., Li, H.J., Fan, J.J., Ju, Y.W., Wang, T.K., Li, X.S., Wu, Y.D., 2012. Structure and coalbed methane occurrence in tectonically deformed coals. Sci. China Earth Sci. 55 (11), 1755–1763.

Jian, K., Fu, X., Ding, Y., Wang, H., Li, T., 2015. Characteristics of pores and methane adsorption of low-rank coal in China. J. Nat. Gas Sci. Eng. 27, 207–218.

Jiang, B.Y., Lin, B.Q., Wu, H.J., Zhu, C.J., Lu, Z.G., 2010. Structural characteristics and fractal laws research in coal and rock ultrafine pore. J. Hunan Univ. Sci. Technol. 25 (3), 17–30 (In Chinese).

Keshavarz, A., Sakurovs, R., Grigore, M., Sayyafzadeh, M., 2017. Effect of maceral composition and coal rank on gas diffusion in Australian coals. Int. J. Coal Geol. 2017 (173), 65–75.

Laxminarayana, C., Crosdale, P.J., 1999. Role of coal type and rank on methane sorption characteristics of Bowen Basin, Australia coals. Int. J. Coal Geol. 40, 309–325.

Lamberson, M.N., Bustin, R.M., 1993. Coalbed methane characteristics of Gates Formation coals, northeastern British Columbia: effect of maceral composition. AAPG Bull. 77 (12), 2062–2076.

Laxminarayana, C., Crosdale, P.J., 2002. Controls on methane sorption capacity of Indian coals. AAPG Bull. 86 (2), 201–212.

Liu, S.Q., Sang, S.X., Liu, H.H., Zhu, Q.P., 2015. Growth characteristics and genetic types of pores and fractures in a high-rank coal reservoir of the southern Qinshui basin. Ore Geol. Rev. 64, 140–151.

Li, A., Ding, W., He, J., He, J., Dai, P., Yin, S., Xie, F., 2016. Investigation of pore structure and fractal characteristics of organic-rich shale reservoirs: a case study of Lower Cambrian Qiongzhusi formation in Malong block of eastern Yunnan Province, South China. Mar. Petrol. Geol. 70, 46–57.

Mavor, M.J., Owen, L.B., Pratt, T.J., 1990. Measurement and evaluation of coal sorption isotherm data. In: SPE Annual Technical Conference and Exhibition. Society of Petroleum Engineers.

Meng, Z., Liu, S., Li, G., 2016. Adsorption capacity, adsorption potential and surface free energy of different structure high rank coals. J. Petrol. Sci. Eng. 146, 856–865.

Menon, P.G., 1968. Adsorption at high pressures. Chem. Rev. 68 (3), 277–294.

Peng, C., Zou, C., Yang, Y., Zhang, G., Wang, W., 2017. Fractal analysis of high rank coal from southeast Qinshui basin by using gas adsorption and mercury porosimetry. J. Petrol. Sci. Eng. 156, 235–249.

Wang, K., Fu, X., Qin, Y., Sesay, S.K., 2011. Adsorption characteristics of lignite in China. J. Earth Sci. 22 (3), 371–376.

Wang, K., Wang, G., Ren, T., Cheng, Y., 2014. Methane and CO_2 sorption hysteresis on coal: a critical review. Int. J. Coal Geol. 132, 60–80.

White, C.M., Smith, D.H., Jones, K.L., Goodman, A.L., Jikich, S.A., LaCount, R.B., DuBose, S.B., Ozdemir, E., Morsi, B.I., Schroeder, K.T., 2005. Sequestration of carbon dioxide in coal with enhanced coalbed methane recovery a review. Energy Fuels 19 (3), 659–724.

Ye, X., Chen, C.F., Jiang, W.L., Deng, H., Xu, C., 2009. Geological characteristics and new development progress of low rank seam coalbed methane in China. Coal Sci. Technol. 8, 111–115.

Yee, D., Seidle, J.P., Hanson, W.B., 1993. Chapter 9. Gas Sorption on Coal and Measurement of Gas Content, 38, pp. 203–218.

Zhao, D.F., Guo, Y.H., Xie, D.L., Su, C., Yang, Y.J., Yu, Y.F., 2014. Fractal characteristics of pores in shale reservoirs based on low temperature nitrogen adsorption experiments. J. Northeastern Petrol. Univ. 38 (6), 100–108 (In Chinese).

Zhou, S., Liu, D., Cai, Y., Yao, Y.B., Che, Y., Liu, Z.H., 2017a. Multi-scale fractal characterizations of lignite, subbituminous and high-volatile bituminous coals pores by mercury intrusion porosimetry. J. Nat. Gas Sci. Eng. 44, 338–350.

Zhou, S., Liu, D., Cai, Y., Yao, Y.B., 2017b. Effects of the coalification jump on the petrophysical properties of lignite, subbituminous and high-volatile bituminous coals. Fuel 199, 219–228.

Zhang, Z., Qin, Y., Wang, G.X., Fu, X., 2013. Numerical description of coalbed methane desorption stages based on isothermal adsorption experiment. Sci. China 56 (6), 1029–1036.

Zhang, S., Tang, S., Tang, D., Yan, Z., Zhang, B., Zhang, J., 2009. Fractal characteristics of coal reservoir seepage Pore, East margin of Ordos Basin. J. China Univ. Min. Technol. 38 (5), 713–718.

Zhang, S., Tang, S., Tang, D., Huang, W., Pan, Z., 2014. Determining fractal dimensions of coal pores by FHH model: problems and effects. J. Nat. Gas Sci. Eng. 21, 929–939.